Proprioceptive integration in motor control*

Erik Skjoldan Mortensen and Mark Schram Christensen

Department of Psychology, University of Copenhagen
Øster Farimagsgade 2A, Copenhagen, Denmark

Abstract

Muscle vibration alters both perceived limb position and velocity by increasing type Ia afferent firing rates, although these afferents mainly encode velocity. Predictive frameworks of sensori-motor control, such as Active Inference and Optimal Feedback Control, suggest that velocity signals should inform position estimates. Such a function would predict that errors in perceived limb position and velocity should be correlated, but this prediction remains empirically underexplored. We hypothesized that an online evaluation of the integral of sensed velocity influences the perceived arm position during active movements. Using a virtual reality-based reaching task, we investigated how vibration-biased proprioceptive feedback influences voluntary movement control. Our results suggest that muscle vibration biases perceived movement velocity, with downstream effects on perceived limb position and reflexive corrections of movement speed. We found that (i) antagonist vibration during active movement caused participants to both overestimate their movement speed while also slowing down, (ii) movement speed and endpoint errors were correlated, with muscle vibration affecting both, and (iii) adjustments in movement speed to muscle vibration are sufficiently fast to be reflexive. Together, these findings support the hypothesis that proprioceptive velocity signals are integrated to augment inference of position, consistent with predictive frameworks of sensorimotor control.

1 Key points

- During movement without visual feedback, the central nervous system (CNS) has access to both position- and velocity-based proprioceptive signals, which are used to estimate limb state.
- Muscle vibration biases the perception of limb position, as seen in the classically observed pattern of biased endpoint errors, through the stimulation of primary (type Ia) muscle spindles, a velocity sensor.
- We investigated how proprioceptive velocity signals affect position estimation during movement by applying muscle vibration while measuring perceived movement speed, actual movement speed, and endpoint errors in a virtual reality (VR) based reaching task.
- We show that errors in perceived limb position and velocity are correlated during active movements, consistent with predictive frameworks of sensorimotor control.
- These findings support the idea that the CNS maintains a self-consistent estimate of limb state across both position and velocity domains.

*This manuscript was first published as a preprint: Erik Skjoldan Mortensen, Mark Schram Christensen (2025). *Proprioceptive integration in motor control.* bioRxiv. https://doi.org/10.1101/2025.07.18.665517.

2 Introduction

To reach out and grasp an object, we must infer our own body position and movement kinematics. If we plan for our hand to arrive at a specific end position with a particular velocity (e.g., zero), the action required to achieve this must account for the hand's position and velocity as it is moving towards the target. Central to this task is the continuous stream of sensory information processed by the CNS, with vision and proprioception being the most relevant for a reaching task. While vision is not necessary (we can reach a target without looking at our hand), the sense of proprioception continuously supplies the CNS with information regarding the arm's movement parameters.

This proprioceptive information is incorporated into motor control at several different hierarchies in the CNS, with corresponding types of possible movement corrections. These range from short-latency reflexes typically seen in the 20-45 ms range (in the upper limbs), through long-latency reflexes at 50-100 ms, with even longer response times being necessary for conscious and deliberate control (Kurtzer, 2015). While relatively simple spinal circuits mainly drive the former, the long-latency reflexes are trans-cortical and show evidence of being coordinated by an internal model of limb dynamics (Yamamoto & Ohtsuki, 1989; Nakazawa et al., 1997; Kurtzer et al., 2008; Kurtzer, 2015; Keyser et al., 2019).

Two of the primary peripheral sensory organs responsible for these reflexes are the type Ia and type II afferent muscle spindles (Proske & Gandevia, 2012). They carry rich information regarding limb movement, allowing decoding of imposed movement patterns (Roll et al., 2004; Albert et al., 2006). The type Ia afferent primarily signals the rate of change in muscle length, i.e., a velocity signal (Roll et al., 2004; Albert et al., 2006), whereas the type II afferent primarily signals muscle length directly, i.e., a positional signal (Roll & Vedel, 1982). In practice, there is likely significant functional overlap between these afferent types, and their encoding of movement further depends on the activity of the parent muscle, and any external load against which they are working (Dimitriou & Edin, 2008; Macefield & Knellwolf, 2018).

While both of these muscle spindle afferents are sensitive to lengthening of the receptor-bearing muscle, the type Ia in particular also responds well to muscle/tendon vibration (Proske & Gandevia, 2012), prompting a large body of experimental research investigating the contents and inference of these proprioceptive signals. At a behavioural level, it has been demonstrated that the vibration of a muscle can bias both perceived limb position as well as limb velocity (Eklund, 1972; Goodwin et al., 1972; Roll & Vedel, 1982; Gilhodes et al., 1986; Inglis & Frank, 1990). One of the primary techniques for investigating this phenomenon involves vibrating the muscles of a stationary limb and tasking the research participants with mirroring the perceived movement with the contralateral limb. Although researchers have explained their findings in terms of either biased perception of limb position or velocity, it proves challenging to design experiments that allow for distinctive reports of perceived limb velocity, without also inherently reporting changes in limb position, and vice versa. In all cases, the induced bias, whether in dynamic joint movement or a change in a statically sensed position, is perceived to be in the direction that would have resulted from stretching out the vibrated muscle, with the amplitude of the induced bias being positively correlated to vibration amplitude (Roll & Vedel, 1982; Calvin-Figuière et al., 1999). Even complex illusions of limb movement have been demonstrated by "playing back" microneurographically recorded Ia afferent firing patterns through vibration, allowing subjects to recognise specific movement patterns (Albert et al., 2006). This suggests that joint and limb movement are inferred from the combined signalling of afferents from all the muscles involved in controlling said joint.

Similar effects are observed during active movements, when vibration is applied to the antagonist

(passively lengthening) muscle. Here, antagonist vibration causes a bias towards undershooting presented visual targets, when moving without visual feedback of the hand (Capaday & Cooke, 1981). Moreover, when vibration is applied to a larger portion of the movement, the target is undershot to a larger degree, indicating a cumulative effect (Cody et al., 1990). Conversely, vibration applied to the agonist (actively contracting) muscle during active movement causes little to no effects (Capaday & Cooke, 1981, 1983; Cody et al., 1990; Inglis & Frank, 1990; Macefield & Knellwolf, 2018).

These behavioural findings align with microneurographic studies of type Ia afferent activity. At rest, type Ia afferents exhibit minimal firing rates, with firing rate increasing proportionally to the velocity of muscle lengthening (Matthews, 1963; Roll & Vedel, 1982; Roll et al., 1989). During muscle shortening in the contracting muscle, the firing rate decreases below baseline, potentially going completely silent (Roll & Vedel, 1982; Macefield & Knellwolf, 2018). The already low baseline activity creates a natural limit on both the amount and precision of information that can be conveyed through further rate reduction. Consequently, with its wider dynamic range of firing rates, the lengthening muscle has been assumed to function as the primary source of joint position/velocity information during active movement, explaining the previously observed limited effects from vibration of the agonist muscle (Capaday & Cooke, 1981).

Electromyographic (EMG) recordings during active movements have shown changes in muscle activity with onset latencies of 40-60 ms (Capaday & Cooke, 1983; Cody et al., 1990). This suggests that a medium-short feedback loop is involved in controlling the relevant muscles in response to Ia afferent feedback. However, no similar latency analysis has been conducted to determine the time course of actual movement speed correction.

In summary, previous research has established that type Ia afferents primarily encode muscle velocity, while type II afferents are more directly associated with static muscle length. However, the behavioral responses to muscle vibration suggest that both perceived limb velocity and position are affected, indicating that proprioceptive state estimation is an integrated process. Specifically, velocity signals from type Ia afferents may inform perceived limb position, contributing to a self-consistent internal estimate of limb state. This kind of cross-modal sensory inference is consistent with predictive frameworks of sensorimotor control, such as Active Inference and Optimal Feedback Control. While these frameworks differ in their formulation, both assume that position and velocity signals derive from a shared underlying state and must remain congruent. For example, if the arm is perceived to be stationary (zero velocity), then its position should not be changing; conversely, a change in position implies a corresponding velocity. This internal consistency is a basic requirement of any dynamic state estimator, and is reflected in these frameworks (Wolpert et al., 1995; Todorov & Jordan, 2002; Friston et al., 2010). Despite these theoretical predictions, the extent to which proprioceptive velocity signals shape position estimation remains empirically unexplored.

In this paper, we investigate how sensed limb position and limb velocity are integrated into a cohesive perception of limb state and movement. Our study is structured around three interrelated research questions:

1. How are changes in perceived and actual movement speed related?
2. How does muscle vibration affect endpoint errors, movement speed, and movement time?
3. What is the latency of movement correction in response to muscle vibration?

Addressing these questions will enhance our understanding of how positional and velocity signals

are integrated for limb state estimation during active movements. To explore these, we designed three VR-based tasks, which are used in conjunction with muscle vibration.

3 Methods

The experiment was conducted at the Department of Psychology, University of Copenhagen, and approved by the local ethics board at the department (no. IP-EC-030723-01). Seventeen healthy participants (3 men, 14 women, all right-handed) were included, with a mean age of 23.4 y (range 20-31 y). All participants provided written and informed consent before participating in the experiment and were compensated monetarily for their time.

3.1 General experimental procedures

A total of three tasks were performed in a single session lasting approximately two hours, sharing the common setup seen in Figure 1. Subjects were seated and had their right arm placed on a rotating armrest, and were outfitted with a VR headset and vibration motors (described in detail in the sections below). With the arm resting on the rotating armrest and holding the attached right VR controller, participants could freely move their arm in the extension and flexion directions with minimal friction. Trials in all tasks were initiated by moving the controller to an indicated start position close to the chest, with the right elbow flexed. Here, subjects would press a thumb key on the controller to indicate their readiness to start, which would change the color of a presented target (semi-transparent sphere with radius of 2.5 cm) from red to yellow. After a short delay (500-1000 ms), the target would turn green, which served as the 'go' signal. Up to this time, a virtual representation of the rotating armrest was visible in the VR environment and was mapped to the actual armrest location. Before each of the three tasks, 10 practice trials were performed.

3.1.1 Task 1

During Task 1, subjects were presented with a target per trial, positioned along a 40-80 ° arc in the extension direction from their starting position. The virtual arm remained visible throughout the movement, but its movement speed was randomized to one of five conditions:

- 12% slower, 6% slower, True speed, 6% faster, or 12% faster

The position of the virtual arm would match that of the real arm at the start of each trial, with a cumulative spatial discrepancy developing over the course of the movement for each of the four manipulated conditions. The virtual arm was hidden during the return movement between each trial. Participants simply needed to move the virtual arm past the target location to end each trial, and were instructed to pay attention to their movement speed. They were informed that the virtual arm was manipulated always to be slightly slower or faster than the actual speed of their arm (they were not informed of the 'True speed' control condition), and they were instructed to judge whether the movement speed of the virtual arm was 'Faster' or 'Slower' than their actual arm after each trial. The above setup was combined with the following four vibration conditions, which started upon arm movement and lasted until the target was reached:

- Agonist vibration, Antagonist vibration, Double vibration, or No vibration

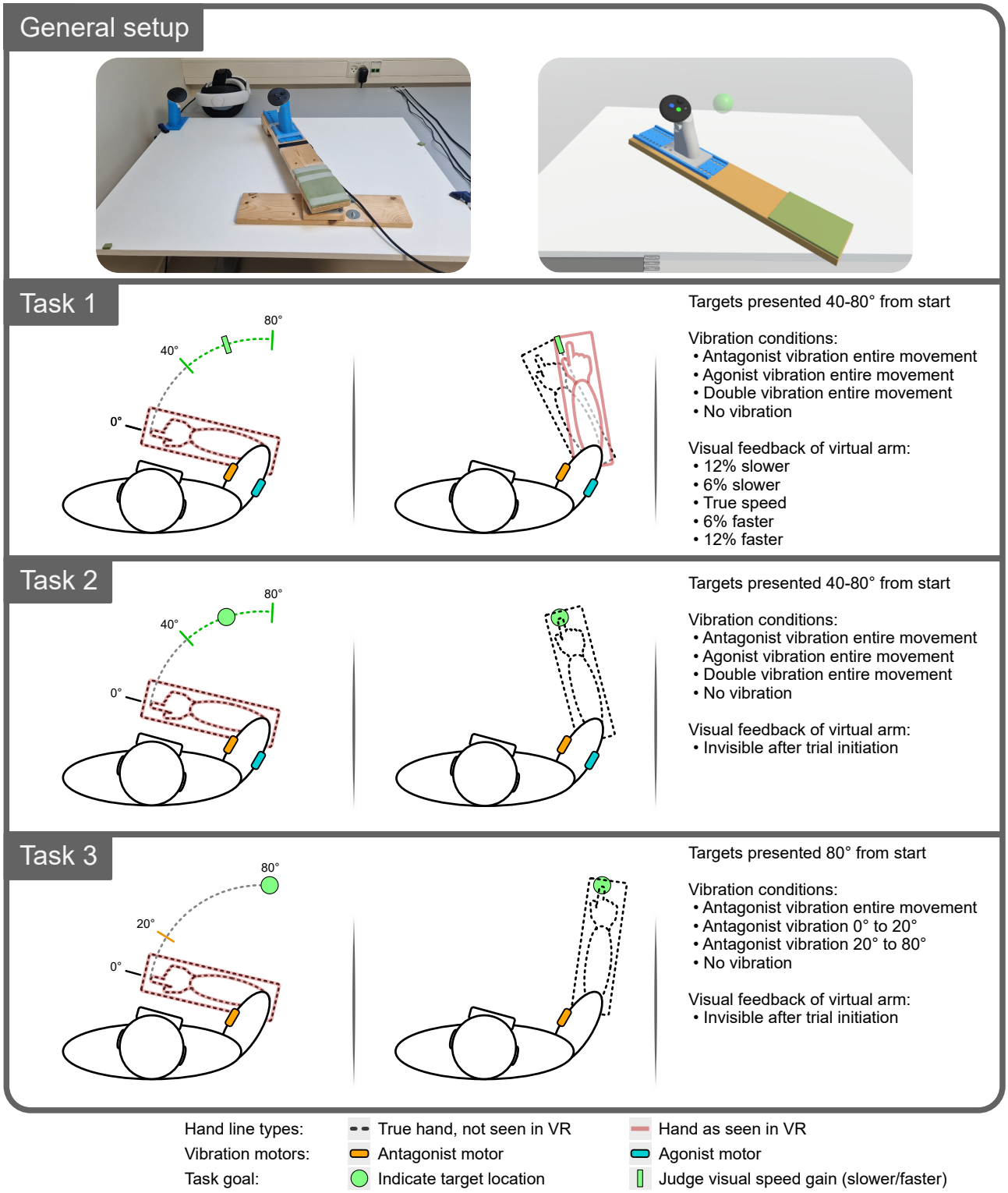

Figure 1: The top panel shows the physical setup on the left and the VR representation that subjects see on the right, here incl. an example target (green sphere). The remaining three panels summarize the experimental setup.

Each visual speed gain and vibration condition was repeated 18 times for a total of 360 trials per participant, split across two runs to allow for a break in between, in a pseudo-randomized order, with a uniform distribution of target distances. The goal of this task was to investigate changes in both actual and perceived movement speed in response to muscle vibration. To the extent that muscle vibration affects the perceived movement speed, this should be reflected in changes in the distribution of reports of the relative speed of the virtual arm.

3.1.2 Task 2

During Task 2, targets were presented 40-80 ° from the starting position. Participants were instructed to indicate the location of the target by moving their arm and pressing a thumb button. Upon the 'go' signal (target turning green), the virtual arm became invisible, leaving only the tabletop and the target visible in the VR environment. Upon movement onset, one of four vibration conditions was started and lasted until the target location was indicated:

- Agonist vibration, Antagonist vibration, Double vibration, or No vibration

The order of vibration conditions was pseudo-randomised, ensuring 24 repetitions of each condition for a total of 96 trials, with a uniform spread of distances to the target. This task was repeated in the flexion direction, starting with the right arm at close to full extension and moving towards the chest for 96 more trials. Our goal with this task was to investigate the effects of muscle vibration on movement speed, time, and endpoint errors.

3.1.3 Task 3

During this task, subjects were again instructed to indicate the target position as precisely as possible, which was here always presented 80 ° from the start location. At trial start, the virtual arm would again turn invisible. To investigate online changes in movement speed in response to turning the antagonist vibration motor on or off during movement, four conditions were used. These are in two sets of intervention-control pairs:

- Vibration 0-20 ° compared to Vibration 0-80 °
- Vibration 20-80 ° compared to No vibration

48 trials of each condition were completed in a pseudo-randomized order, totaling 192 trials per subject.

3.2 Rotating armrest

An armrest allowing rotation around a vertical axis was constructed to support the participant's arm during the experiment. The armrest was positioned so that it had an axis of rotation under the participant's right elbow joint, with the height adjusted to just below the shoulder, thereby minimizing movements of other joints. A smooth tabletop combined with felt sliders on the underside of the armrest allowed for very low-friction movement. The right-hand VR controller was mounted on the armrest, with its exact positioning individualized according to forearm length. The controller provided the necessary button input for the experiment, as well as real-time tracking of the rotating armrest. See figure 1A for visualization.

3.3 VR setup

The experiment was programmed in the Unity engine (v21.3.24f1, Unity Technologies, San Francisco, USA), utilizing the Unity Experiment Framework (Brookes et al., 2020) to control the trial and block structure of the experiment. We used a Meta Quest 3 VR headset (Meta Platforms Technologies Ireland Limited, Dublin, Ireland) connected to the experiment PC via USB Quest Link, allowing the Unity executable to run on the experiment PC and be displayed in the Quest headset. The headset was set up to run at a refresh rate of 90 Hz. The left controller was mounted at the corner of the tabletop, allowing the table to be tracked and displayed in VR, providing participants with a stable visual reference of the working environment.

3.4 Vibration motors

Two small vibration motors (Vp216 VIBRO transducer, Acouve Laboratory Inc., Tokyo, Japan) were mounted on the right arm, with inelastic micropore tape. One was mounted over the distal triceps tendon, just proximal to the elbow, while the other was mounted centrally on the belly of the biceps muscle. This mounting of the biceps motor over the muscle belly rather than the tendon was chosen to minimize changes in mounting pressure due to elbow flexion/extension. Previous research has indicated no difference in the required vibration amplitude to elicit an illusory movement between the distal biceps tendon and the biceps muscle belly (Ferrari et al., 2019).

The vibration motors were controlled by an 80 Hz sine wave audio signal produced by the experiment PC's sound card, with the signal amplified by a stereo PAM8610 amplifier (Diodes Incorporated, Plano, Texas) using a 12 V 1.5 A power supply. The delay from triggering vibration in the experiment software to actual vibration start was determined (118.8 ms (SD = 4.6)) using an Arduino Uno R3 (Arduino S.r.l., Monza, Italy) analogue-to-digital listener, and was accounted for in the timing-sensitive analysis of Task 3.

3.5 Data processing and statistical modeling

Data analysis was conducted in `R` (v4.3.3, R Core Team, 2024) with data wrangling and plotting completed using the `tidyverse` package (v2.0.0, Wickham et al., 2019). Model fitting was performed using the `brms` package (v2.20.4, Bürkner, 2017), an `R` interface for the probabilistic programming language `Stan` (v2.32.6, Stan Development Team, 2024), and the `PyMC` library (v5.10.2, Abril-Pla et al., 2023), in `Python` (v3.7.11, Python Software Foundation, 2023). All models employed weakly informative priors with effect parameters centered at zero, providing mild regularization while allowing the data to dominate the posterior estimates. Hierarchical models with partial pooling were used to account for the nested structure of research participants. Inference was performed using the No-U-Turn Sampler, a variant of Hamiltonian Monte Carlo. All models were run with four independent chains of 4000 iterations each, including 1000 warm-up iterations, yielding 12,000 post-warm-up samples. Convergence diagnostics indicated no divergent transitions, all $\widehat{R}$ values were below 1.005, and caterpillar plots were visually inspected for convergence and mixing.

Posterior distributions for relevant parameters are summarized using the Maximum a Posteriori (MAP) estimate and associated 95% Credible Intervals (CI). An effect was interpreted as supported when the 95% CI did not include zero. All fitted traces, including complete sets of posterior distributions, are made available in the code repository (see the Data Availability section).

All position and velocity data are presented as angular values of the elbow joint.

3.5.1 Task 1

In Task 1, we investigate the effect of muscle vibration on the perceived and actual movement speed. Both models for these two analyses were implemented in brms as hierarchical (multilevel) models with the random effects defined at the participant level. The formula syntax presented follows the structure used for brms, which adheres to the same scheme as that employed in the `lme4` `R` package and is widely adopted in mixed-effects modeling.

To investigate whether the vibration motors influence perceived movement speed, we model the distribution of ratings of 'Faster' and 'Slower' responses. This was done with a Bernoulli model with a probit link, implemented in brms as shown in model 1.

This model assumes that the answer distribution for each condition can be approximated by a latent, z-normalized Gaussian distribution, with a static threshold defining whether 'Faster' or 'Slower' is selected, with this outcome here represented by `rating`. The control, no-vibration condition with an unperturbed speed of visual feedback, is used here as the reference category, with μ set to 0 and σ set to 1 on the latent scale. The parameter estimates of the predictors and the threshold are then modeled relative to this. Agonist (`ago_v`) and antagonist (`anta_v`) vibration are included as predictors, which can increase or decrease μ, to the extent that different rating distributions are observed when muscle vibration is applied. Visual gain (`vg`) is included as a linear predictor, likewise affecting μ of the latent distribution, dependent on the changes in rating distribution. `id` is a unique identifier per participant, indicating that the model is fitted as a multilevel model with shrinkage, which reflects the participant structure of the data.

$$\begin{aligned} \texttt{rating} &\sim 1 + \texttt{vg} + \texttt{ago_v} + \texttt{anta_v} + \\ &\qquad (1 + \texttt{vg} + \texttt{ago_v} + \texttt{anta_v} \mid \texttt{id}) \\ \texttt{family} &= \texttt{bernoulli(link = "probit")} \end{aligned} \tag{1}$$

Additionally, we model the effects on the actual mean movement speed of each trial, as shown in model 2. Here, `mms` (in °/s) represents the mean movement speed of each trial. `mms` was centered by the mean of the no-vibration normal visual feedback condition within-participant, as we are here specifically interested in movement speed changes in response to muscle vibration, and not subject-to-subject variation in baseline movement speed. Here we additionally include the target distance (`td`) as a predictor, as this variable is highly predictive of movement speed.

$$\begin{aligned} \texttt{mms} &\sim 1 + \texttt{vg} + \texttt{ago_v} + \texttt{anta_v} + \texttt{td} + \\ &\qquad (1 + \texttt{vg} + \texttt{ago_v} + \texttt{anta_v} + \texttt{td} \mid \texttt{id}) \\ \texttt{family} &= \texttt{gaussian()} \end{aligned} \tag{2}$$

360 trials were completed per participant, except for one, for whom the last 194 trials could not be completed due to technical issues. This leaves a total of 5926 included trials.

3.5.2 Task 2

To investigate how the sensorimotor system integrates the afferent proprioceptive feedback, we model endpoint errors (`epe`, in °), mean movement speed (`mms`, in °/s), and movement time (`mt`, in s) during

Task 2 as outcomes in a hierarchical multivariate model. This was implemented in brms, as shown in model 3.

Prior to model fitting, the data were centered by the mean in the no-vibration condition within each participant, for each outcome. Beyond aiding model convergence, this enables us to estimate how each vibration condition affects the three outcome variables, relative to the case when no vibration is present; we are here interested in how, e.g., endpoint error accuracy changes in response to muscle vibration, while accounting for any individual baseline inaccuracy. Apart from the vibration conditions (*ago_v* and *anta_v*), we also include the distance to the target (*td*), to account for baseline differences in endpoint errors, movement speed, and movement time that depend on the distance to the target. Additionally, the movement direction (*md*) and its interactions with vibration and target distance variables are included to differentiate between effects observed for flexion and extension movements. This also accounts for the fact that the biceps muscle functions as the antagonist muscle during extension but as the agonist muscle during flexion, and vice versa for the triceps. An interaction term between the two muscle vibrations is also included here to investigate the extent to which the combination of both vibration motors has different effects than the sum of the effects of each type of muscle vibration alone.

$$
\begin{aligned}
\texttt{epe},\ \texttt{mms},\ \texttt{mt} &\sim 1 + \texttt{ago_v} \cdot \texttt{anta_v} + \cdot\texttt{md} + \texttt{td} \cdot \texttt{md} + \\
&\quad (1 + \texttt{ago_v} \cdot \texttt{anta_v} \cdot \texttt{md} + \texttt{td} \cdot \texttt{md} \mid \texttt{id}) \\
\texttt{sigma} &\sim 1 + \texttt{ago_v} \cdot \texttt{anta_v} \cdot \texttt{md} + \\
&\quad (1 + \texttt{ago_v} \cdot \texttt{anta_v} \cdot \texttt{md} \mid \texttt{id}) \\
&\quad + \texttt{set_rescor(TRUE)} \\
\texttt{family} &= \texttt{gaussian()}
\end{aligned} \tag{3}
$$

A total of 192 trials (96 per direction) were included for each participant, resulting in 3264 trials.

3.5.3 Integrative analysis of Tasks 1 & 2

A further analysis of Tasks 1 and 2 was completed, using only the baseline control trials from each task, i.e., a subset of the data also used for the analyses described in the above two sections. Specifically, trials with no visual speed gain and no vibration were included from Task 1, while trials with no vibration were included from Task 2.

Model 4 shows the `brms` syntax used to fit the follow-up analysis on the subset trials from Task 1. This model shares the same Bernoulli (probit-link) structure as the first model described for Task 1; however, here we examine whether movement speed predicts the tendency to overestimate or underestimate perceived movement speed. `rating` refers to whether the virtual arm was rated as 'Faster' or 'Slower'. To account for between-subject differences in both the mean and variability of movement speed, the predictor was z-normalized within each participant prior to model fitting (denoted as `mms_zn`).

$$
\begin{aligned}
\texttt{rating} \sim 1 + \texttt{mms_zn} + \texttt{td} + \\
(1 + \texttt{mms_zn} + \texttt{td}) \\
\texttt{family} = \texttt{bernoulli(link = "probit")}
\end{aligned} \tag{4}
$$

Model 5 shows syntax used for the Task 2 subset trials. Here we investigate the extent to which movement speed is predictive of endpoint errors. Here, both the endpoint errors and mean movement speed are likewise z-normalized (`epe_zn` and `mms_zn`) to account for between-subject differences as above.

$$
\begin{aligned}
\texttt{epe_zn} \sim 1 + \texttt{mms_zn} \cdot \texttt{md} + \texttt{td} \cdot \texttt{md} + \\
(1 + \texttt{mms_zn} \cdot \texttt{md} + \texttt{td} \cdot \texttt{md} \mid \texttt{id}) \\
\texttt{family} = \texttt{gaussian()}
\end{aligned} \tag{5}
$$

`td` refers to the target distance and is included in both models to capture any effect of varied target distances on the respective outcomes. `md` refers to movement direction and is included in the second model to differentiate between flexion and extension direction movement.

3.5.4 Task 3

To investigate the latency from the antagonist vibration motor turning on and off, respectively, until a compensatory change in movement speed could be observed, we implemented a changepoint model (e.g., see (Carlin et al., 1992)) in PyMC. To effectively run the model, some preprocessing of the tracking data was required. First, the time t was adjusted to be set to 0 at the time of starting/stopping the vibration motor, which was triggered at 20 ° into the movement. Data from 100 ms before to 120 ms after vibration start/stop was included in the model fitting. The raw tracking data was position-based, and to estimate angular movement speed, we used the first derivative of a cubic smoothing spline applied to the angular position data, using `R` 's `smooth.spline()` function with the smoothing parameter (`spar`) set to 0.4. The movement speed was extracted at 10 ms intervals, which was then used in the changepoint model as follows.

The mean movement speed at each time point t_i was calculated across trials within each control condition ('No vibration' and 'Antagonist vibration 0-80 °'), within-participant. These mean values were then subtracted from the trial-level movement speed data, at each time point t_i, in the corresponding intervention condition ('Vibration 20-80 °' and 'Antagonist vibration 0-20 °'). After this step, the data represent the timeline of delta movement speed in each intervention condition trial, compared to the mean movement speed at each time point in the corresponding control condition for that participant.

The mean of this delta movement speed should now be close to zero until vibration start/stop begins to affect the movement speed in the intervention condition, at which point the delta movement speed should then begin to diverge away. The changepoint model is set up to estimate this time point. To see a visualization of this, along with the fitting process, see figure A2 in the appendix.

For simplicity, only the model likelihood, along with the priors of the changepoint, is shown here in formula 6. dms_i is the delta movement speed at time t_i. The model uses this to sample the most likely time of change in movement speed (group mean changepoint denoted $\overline{\tau}$, participant to participant SD

denoted τ_σ) given the model formulation below. To allow for sampling of a continuous changepoint, we use the value of a sigmoid function (S_i at t_i) to blend smoothly between the pre- and post-changepoint linear functions. A uniform prior for the group mean changepoint was used, between 0 ms (vibration start/stop) and +120 ms. The same model, including identical priors, was run twice, once each for the two sets of intervention-control pairs of conditions. The complete model definition with all priors may be found in the appendix (model A1), where it is also described in further detail.

$$
\begin{aligned}
dms_i &\sim \mathcal{N}(\mu_i, \sigma_j) \\
\mu_i &= \mu_pre_\tau_i \cdot S_i + \mu_post_\tau_i \cdot (1 - S_i) \\
S_i &= \frac{1}{1 + e^{\frac{t_i - \tau_j}{0.001}}} \\
\mu_pre_\tau_i &= \alpha_pre_\tau_j + \beta_pre_\tau_j \cdot t_i \\
\mu_post_\tau_i &= \alpha_post_\tau_j + \beta_post_\tau_j \cdot t_i \\
\tau_j &= \overline{\tau} + \tau_\sigma \cdot \epsilon_\tau_j && \text{for } j \in \{1, \ldots, n_{id}\} \\
\epsilon_\tau_j &\sim \mathcal{N}(0, 1) && \text{for } j \in \{1, \ldots, n_{id}\} \\
\overline{\tau} &\sim \mathcal{U}(0, t_{max}) \\
\tau_\sigma &\sim \mathrm{HN}(0.025)
\end{aligned}
\tag{6}
$$

48 trials of each of the four conditions per 17 subjects (816 per condition) were completed during data collection. However, a small number of trials were excluded due to transient tracking issues. A total of 16 trials were discarded across the four conditions. Data from -100 ms before to 120 ms after vibration start/stop was included, at 10 ms intervals for 23 observations per trial.

To test whether the above-mentioned spline method was a reasonable approach for estimating movement speed for this use case, a simple finite-difference approach to estimating angular movement speed was also tested with the same changepoint model. Here, the movement speed was estimated as follows, before being linearly interpolated to align samples temporally:

$$ms_i = \frac{angle_{i+1} - angle_{i-1}}{t_{i+1} - t_{i-1}}$$

Both methods produced group mean latency estimates within 2 ms of each other for both model fits (vibration on and off), while the spline method filtered out some of the noise apparent at the trial level in the finite-differences approach. Both sets of estimated movement speed data and model traces are available at the code and data repository mentioned in the Data Availability section.

4 Results

4.1 Task 1

In Task 1, we investigated the effects of muscle vibration on both the perceived movement speed and the actual movement speed.

As one might expect, the results indicate an approximately 50% probability of rating the virtual arm as 'Faster' in the 'No vibration' condition with no visual speed gain, indicating that the average estimation of relative movement speed is correct. Varying the visual speed gain from -12% to $+12\%$, Figure 2A shows the expected shift in the probability of reporting the virtual arm as 'Faster'; when the visual speed gain is increased, the probability of reporting the virtual arm as 'Faster' increases. This

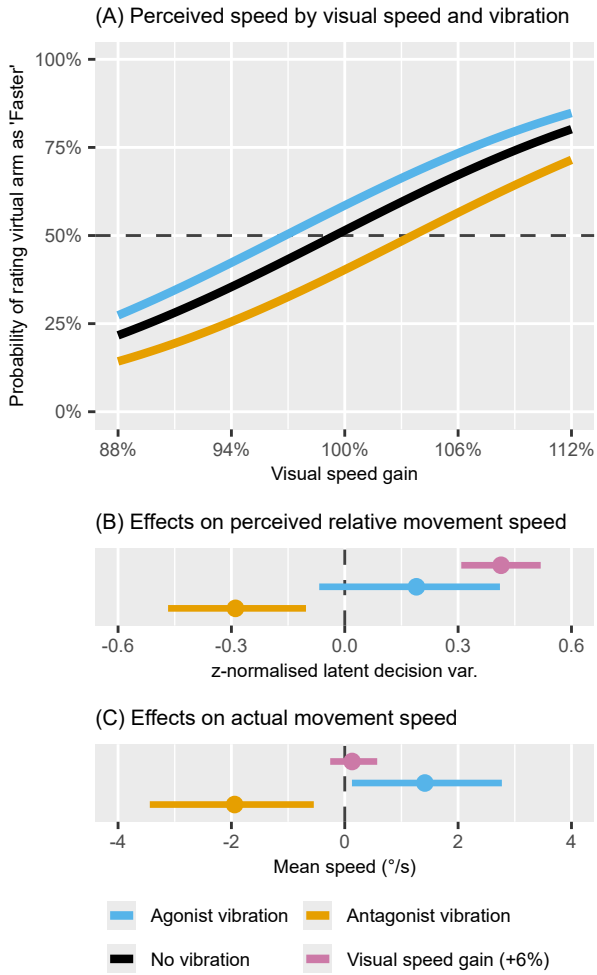

Figure 2: Shows the results of Task 1. Panel A shows the modeled probability of rating visual feedback as appearing 'Faster', for the control 'No vibration' condition (gray), as well as with agonist vibration (teal) and antagonist vibration (orange). Panel B shows the modeled z-normalized latent distribution differences between the agonist and antagonist vibration conditions relative to the 'No vibration' condition. As a point of reference, the modeled effect of increased speed of +6% visual speed gain is also shown. Panel C shows how the same three conditions affect mean movement speed compared to the 'No vibration, normal visual speed' control condition. Dots and point intervals represent maximum a posteriori (MAP) and 95% CI.

effect was estimated with a coefficient of 0.41 (95% CI [0.31, 0.52]) for a visual gain of +6% (purple line interval, Figure 2B). Having thus validated that participants can successfully compare their own arm movement speed to that of the virtual arm, we can interpret the effects of applying muscle vibration during this task. Here, we found a decrease in the probability of reporting the virtual arm as 'Faster' when antagonist vibration is applied, with a coefficient of -0.29 (95% CI [-0.47, -0.1]). This may then be interpreted as antagonist muscle vibration causing participants to overestimate their movement speed, as they here become less likely to report the virtual arm as 'Faster'. For further visualization of the underlying rating data, see Figure A1A in the appendix.

In addition to biasing the perceived movement speed, antagonist vibration also affects the actual movement speed; as participants believe they are moving faster, they decrease their actual mean movement speed by 1.94 °/s (95% CI [0.55, 3.44]).

For agonist vibration, the results are mixed. While the actual movement speed increased by 1.41 °/s (95% CI [0.13, 2.88]), the 95% credible interval describing the change in probability of reporting the

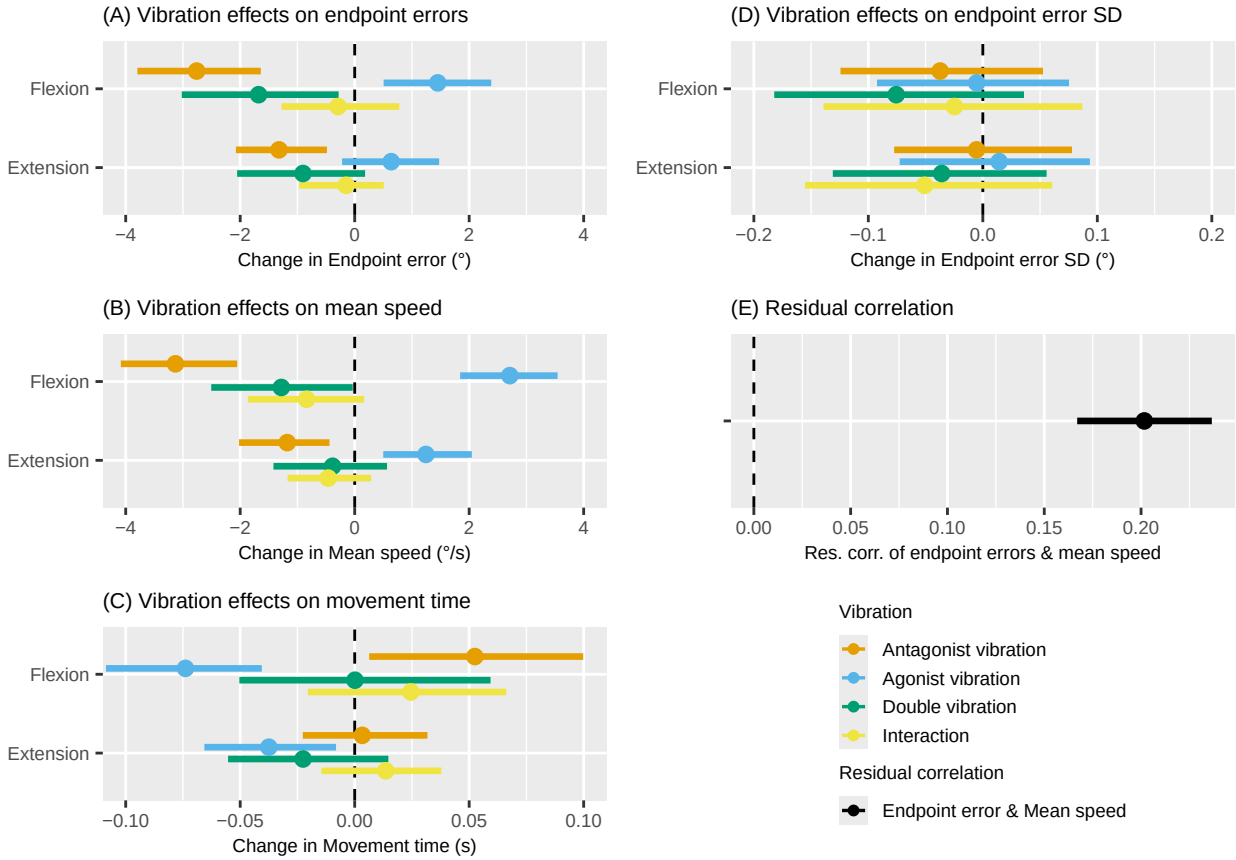

Figure 3: Shows the results of Task 2. Panels A, B, and C show the modeled effects of agonist and antagonist vibration, their interaction, and both together. Effects are shown for flexion and extension movements relative to the control 'No vibration' condition, on Endpoint errors (A), Mean movement speed (B), and Movement time (C), respectively. Negative values indicate undershooting the target, decreased mean movement speed, and decreased movement time, relative to the 'No vibration' condition. Effects are shown conditional on the mean target distance of 60 ° (range 40-80 °). Panel D shows the effects on the change in standard deviation of Endpoint errors relative to the 'No vibration' condition. Panel D shows the modeled residual correlation of Endpoint errors and Mean movement speed. Dots and point intervals represent MAP and 95% CI.

perceived movement speed overlapped 0, indicating insufficient evidence to claim such an effect. Visual speed gain was found not to affect the actual movement speed.

4.2 Task 2

In Task 2, we investigated how muscle vibration affects movement time, movement speed, and endpoint errors (Figure 6). While we focus on the changes in performance caused by muscle vibration in the following section, a summary of the baseline performance in the 'No vibration' trials is provided in Table A1 for reference in the appendix.

We found that antagonist vibration caused a consistent bias towards undershooting the target, both in the flexion (-2.76 ° (95% CI [-3.8, -1.64])) and extension directions (-1.32 ° (95% CI [-2.07, -0.48])). Agonist vibration, in contrast, caused participants to overshoot the target in the flexion direction (1.45 ° (95% CI [0.51, 2.39])), but not in the extension direction. Furthermore, we found no indication of increased standard deviation of endpoint errors, suggesting that neither agonist, antagonist, nor both of them together have any effects on movement precision, but only on accuracy in this task (Figure

3D). The effects of muscle vibration on movement speed presented a very similar pattern of relative effect sizes to those observed for endpoint errors. Antagonist vibration caused a decrease in movement speed (flexion direction: -3.13 °/s (95% CI [-4.09, -2.05]), extension direction: -1.18 °/s (95% CI [-2.02, -0.44])), while agonist vibration resulted in a consistent increase in movement speed (flexion direction: 2.71 °/s (95% CI [1.84, 3.54]), extension direction: 1.25 °/s (95% CI [0.5, 2.05])). Additionally, we found a residual correlation of 0.20 (95% CI [0.17, 0.24], Figure 3D) between movement speed and endpoint errors, indicating that movement speed is predictive of endpoint errors after accounting for the modeled effects of the vibration motors on both parameters.

To further highlight how endpoint error and mean movement speed are affected by muscle vibration, they are plotted against each other in Figure 4. In this plot, endpoint errors and mean movement speed are both z-normalized by the values in the no vibration condition, within each participant, to account for subject-to-subject variation, while highlighting how endpoint errors and mean speed change in response to muscle vibration. Here, it becomes apparent how antagonist vibration pushes the distribution down and to the left, while agonist vibration pushes it up and to the right.

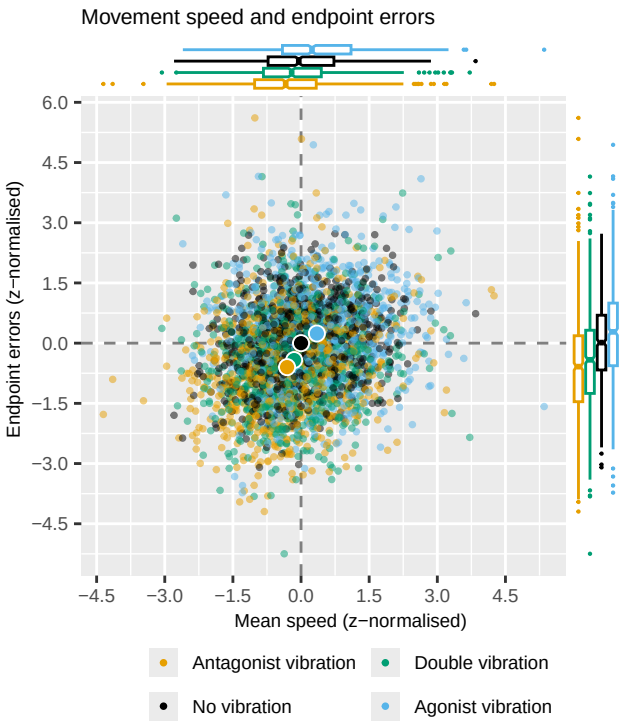

Figure 4: Shows mean movement speed and endpoint errors from Task 2. All values are z-normalized within-subject by the values of the control 'No vibration' condition, to account for subject-to-subject variation in both movement speed as well as endpoint error precision and accuracy. Small dots represent individual trials, while large dots show the mean of each vibration condition. Boxplots show trial distributions along each axis. Both flexion and extension direction trials are included.

Additionally, we found small but consistent effects of muscle vibration on movement time, but in the opposite direction compared to what one might expect, considering the described effects on endpoint errors. In a simplified manner, a change towards undershooting the target due to antagonist vibration may have been caused by either a decrease in movement time at a similar movement speed or a reduction in movement speed at a similar movement time. In contrast to this, we found that antagonist vibration during flexion movement caused a bias towards increased movement time of 52.48 ms (95% CI [6.34, 99.79]), while agonist vibration caused decreases in movement time of -73.9 ms (95% CI [-108.62, -

40.57]) for flexion movements and -37.48 ms (95% CI [-65.65, -8.14]) for extension movements. These changes in movement time effectively work in the opposite direction as the changes in movement speed, in terms of achieving a given endpoint error.

For none of the three outcomes did we find any vibration interaction effects (Figure 3A, B & C), indicating that the impact of concurrent vibration of both the agonist and antagonist motor can be well explained by the sum of their individual effects.

4.3 Integrative analysis of Tasks 1 and 2

One way to jointly interpret the above findings from Tasks 1 and 2 is to assume that the CNS estimates limb position during movement by integrating sensed movement speed over time, as in predictive frameworks of sensori-motor control, and that the base driving effect of muscle vibration acts through biasing the sensed movement speed. In such a framework, the perceived position is, in part, shaped by the ongoing evaluation of velocity signals.

To further evaluate this framework, we tested two predictions based on the following assumptions: (i) movement speed is continually adjusted based on sensed speed, and (ii) perceived speed contributes to perceived position. If true, these relationships should also be evident in non-perturbed trials. Specifically:

1. Movement speed should predict the probability of over- or underestimating one's movement speed. For example, participants who slow down may be compensating for an overestimation of their actual speed.

2. Movement speed should also predict endpoint errors. Overestimating speed would lead to both compensatory slowdown and overestimation of covered distance.

The results of these analyses are reported in Figure 5. Here, Figure 5A shows the predicted effect of z-normalized mean movement speed on the reported perception of movement speed, such that slower movements are associated with overestimation of movement speed (being less likely to report the virtual arm as 'Faster'), and vice versa, with a coefficient of 0.37 (95% CI [0.14, 0.61]). This refers to a change in mu of the modeled latent z-normalized decision variable of 0.37 per standard deviation of z-normalized mean movement speed. We have further provided a plot of the distribution of mean movement speed across the two ratings in Figure A1B in the appendix.

Figure 5B likewise shows the hypothesized positive predictive effect of z-normalized mean movement speed on endpoint errors, with practically identical slopes of 0.27 (95% CI [0.08, 0.46]) for extension movements and 0.27 (95% CI [0.09, 0.47]) for flexion movements.

4.4 Task 3

In Task 3, we adjusted the experimental setup in order to get a more detailed estimate of how the sensori-motor system incorporates information from the Ia afferents in real-time during movement, by turning on or off the antagonist vibration motor 20° into an 80° extension movement.

Figure 6 shows the same two control conditions in both panels A and B, with no vibration in the dashed grey line and antagonist vibration over the entire movement in the fully drawn grey line. Figure 6A shows how turning on the antagonist vibration motor causes subjects to begin decreasing their movement speed at an estimated group mean latency of 48.2 ms (95% CI [42.9, 53.5], with a subject-to-subject standard deviation of 1.0 ms (95% CI [0.2, 9.9]). Similarly, turning off the antagonist

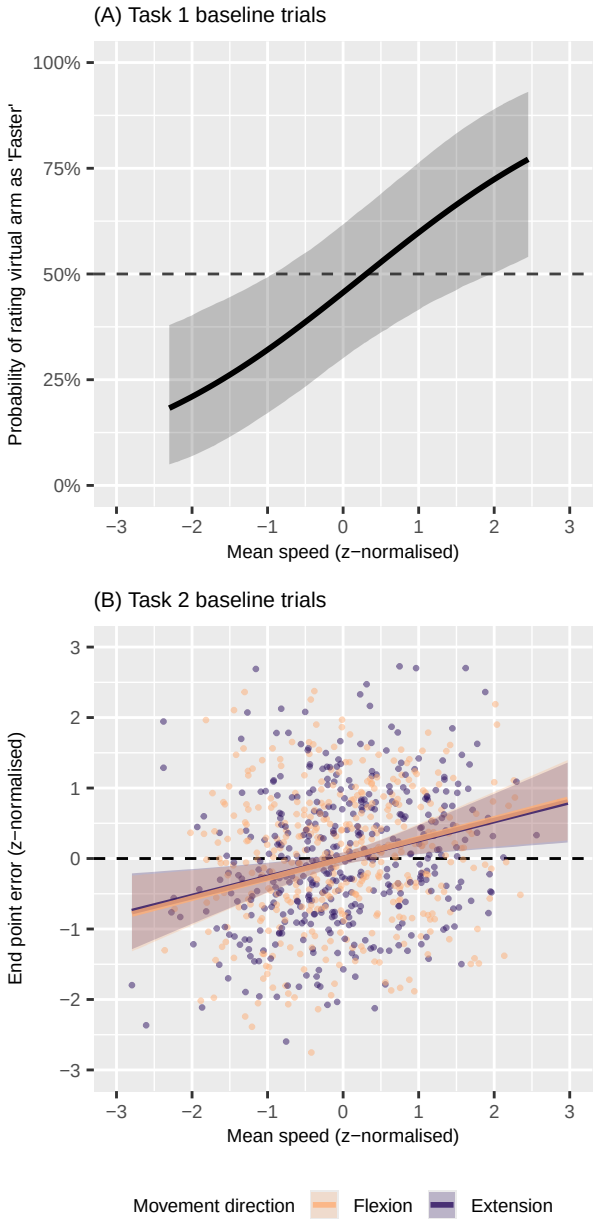

Figure 5: Panel A shows the MAP and 95% CI predicted probability of rating virtual arm as 'Faster' in the subset of trials from Task 1 with 'No vibration & no visual speed gain', dependent on z-normalized mean movement speed. Panel B shows z-normalized (within-subject and direction) mean speed and endpoint errors from the subset of trials with 'No vibration' from Task 2. Dots show individual trials, with overlaid posterior conditional effects linear regression lines showing the MAP and 95% CI.

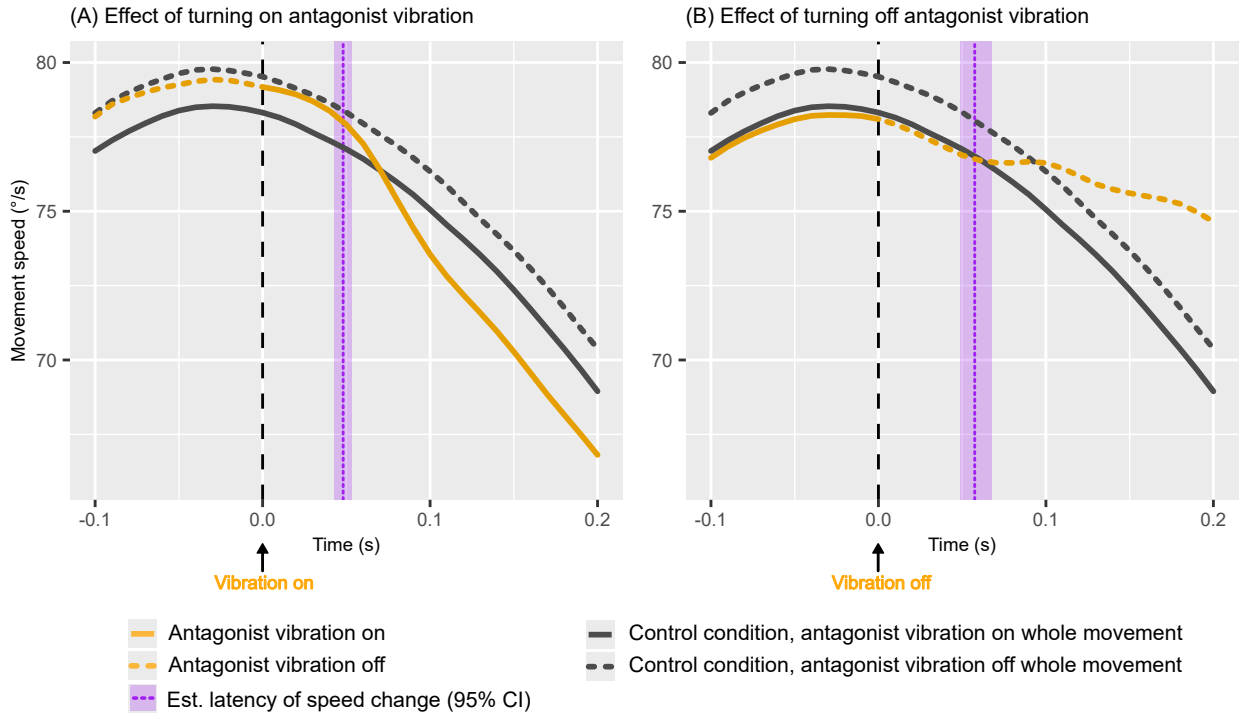

Figure 6: Panels A and B each show how movement speed is affected immediately after turning on (A) and off (B) the antagonist vibration motor 20° into an 80° extension movement. Overlaid is the MAP and 95% CI estimated group mean latency from vibration start/stop until movement speed is affected in purple. Grey lines are used to indicate the two control conditions, with the motor on or off throughout the movement. Orange lines show the intervention conditions, where the motor turns on (A) and off (B) 20° into the movement, time-locked to 0. Dotted line segments indicate when the motor is off, while solid lines indicate when the motor is on. Each line represents the mean movement speed of 816 trials (48 per subject). See model 6 for details of latency estimation.

vibration motor causes subjects to begin increasing their movement speed with a latency of 58.0 ms (95% CI [48.7, 67.7]), and with a subject-to-subject standard deviation of 11.3 ms (95% CI [3.3, 22.8]). In both cases, the change in movement speed is greater than the difference in movement speed between the two control conditions, where antagonist vibration was on or off for the entire movement.

5 Discussion

We set out to investigate how sensed limb position and velocity are integrated into a cohesive perception of limb state and movement. While the individual effects of muscle vibration on endpoint errors, changes in movement speed, and the reportable perception of limb state have all been described in the existing literature, we sought here to provide a comprehensive picture of how these factors interact with one another during active movements.

Our investigation was based on the hypothesis that proprioceptive positional and velocity signals interact in a reciprocally reinforcing manner. Specifically, we explored the prediction that velocity signals contribute to the perceived position of the arm during reaching movements.

In the following subsections, we will discuss the findings from each of the three tasks in turn, addressing the three research questions outlined in the introduction.

5.1 Muscle vibration biases both perceived and actual movement speed

In Task 1, the results show that antagonist muscle vibration causes participants to overestimate their movement speed while simultaneously decreasing their actual movement speed. This suggests that vibration-induced activity of the type Ia afferents biases the perceived movement speed, causing a reactive change in actual movement speed to compensate.

By tasking participants with rating whether the virtual arm had moved faster or slower than their actual arm on each trial, we essentially ask them to compare two measures of movement speed, which, under normal conditions, would likely be combined and integrated in the final perception of limb state. Although this does not necessarily align with the typical sensory integration process, it nonetheless offers insight into how proprioceptive feedback influences the perceived movement speed of self-paced movements.

By further considering our analysis of the subset of trials with no vibration and normal visual feedback, we observe that movement speed is generally predictive of the reported perception of movement speed. Specifically, trials performed with higher movement speeds are associated with underestimating the movement speed of the arm, and vice versa. In a predictive framework of state estimation, both efferent drive and afferent feedback are utilized (Van Beers et al., 2002). Given that it is well understood that muscle vibration actively biases the muscle velocity sensors (Roll & Vedel, 1982; Gilhodes et al., 1986; Roll et al., 2004), and that muscle vibration does affect both perceived and actual movement speed in a similar manner as seen here, it seems likely that the observed baseline association is at least in part driven by spontaneous errors in the perceived movement speed on a trial to trial basis, causing reactive changes in movement speed. Together, these observations support the assumption that movement speed is adjusted in response to perceived movement speed.

The velocity profile of reaching movements is typically bell-shaped and smooth, a feature that has been well-accounted for by models based on signal-dependent noise and Optimal Feedback Control (Harris & Wolpert, 1998; Todorov & Jordan, 1998), as well as through models that minimize variational free energy (Friston et al., 2010). From either of these perspectives, any error in the perception of movement speed, whether arising spontaneously or through muscle vibration, would be expected to trigger the observed compensatory motor adjustments. These may align ongoing movement with either a planned optimal trajectory or with predictions produced by a generative model, depending on the control framework.

5.2 Perceived movement speed biases position estimation

In Task 2, the results mirror those seen in Task 1 in terms of the effects of muscle vibration on movement speed. Building upon the argumentation in the previous section, these effects may similarly be assumed to be in response to an induced bias in the perception of movement speed. The observed changes in movement speed are accompanied by congruent changes in endpoint error, indicating biases in the perceived arm position at the end of the movement. This is seen in that antagonist vibration causes both decreased movement speed and a bias towards undershooting the target. Thus, considering Tasks 1 and 2 together, our results indicate that vibration-induced biases in the perception of movement speed are associated with congruent biases in the perception of limb position. This observation supports the hypothesis that estimation of limb position and velocity is an integrated process, as predicted by both Active Inference (Friston et al., 2010) and Optimal Feedback Control (Wolpert et al., 1995) frameworks.

Over the course of a movement, the integral of sensed velocity becomes an estimate of the total change in position, which in this framework would predict that the sensori-motor system's estimate

of current limb position depends on the pre-movement estimate of limb start position. This pattern has previously been observed in that vision of the hand position pre-movement increases accuracy and precision of endpoint errors (Rossetti et al., 1994; Desmurget et al., 1997), while the endpoint errors of movements with biased perceived starting positions likewise are skewed to indicate that the perceived limb position at the end of the movement is influenced by the initial perceived limb position (Rossetti et al., 1995; Patterson et al., 2017). Both the residual correlation found between movement speed and endpoint errors in the primary analysis of Task 2, as well as the subanalysis including only the 'No vibration' trials, further demonstrate that errors in perceived arm position, observed through endpoint errors, are generally correlated with errors in perceived movement speed, inferred here through variation in movement speed, which indicates a similar pattern.

While we do see some minor changes in movement time in response to muscle vibration, these are consistently in the opposite direction as what might have explained the changes in endpoint errors; e.g., undershooting the target might, in a simplified fashion, have been associated either with moving slower for an unchanged movement time, or moving for a shorter time at a similar speed. Instead, we tend to see increased movement time in response to antagonist vibration, effectively increasing the required decrease in movement speed to achieve the same shift in endpoint error towards undershooting the target.

Finally, we did not find evidence indicating that muscle vibration causes a decrease in endpoint error precision. This observation is somewhat contrary to previous findings, which have indicated that muscle vibration may decrease the precision or weight placed on proprioceptive signals. This has been observed in tasks where antagonist-pair double vibration has been used to increase the strength of visual illusion (Chancel et al., 2016; Chancel & Ehrsson, 2023), which the authors described in terms of decreased relative weighting of proprioceptive feedback in this condition. Additionally, it has been observed that muscle vibration leads to a decrease in the precision of force production (Bock et al., 2007), which would also seem to predict decreased precision of endpoint errors. As such, it is surprising that we observe no effects on precision, but only on accuracy, in the current task.

5.3 Online control of movement speed

In Task 3, results show how movement speed is affected immediately following turning on or off the antagonist vibration motor. The expected decrease in movement speed in response to antagonist vibration had an onset latency of approximately 50 ms. This finding is in line with previous EMG-based research, which has identified changes in muscle activity at latencies of 40-60 ms (Capaday & Cooke, 1983; Cody et al., 1990). Our observations further expand on this work, demonstrating that the previously observed latency of EMG response matches well with actual changes in movement speed, which quickly exceeds the difference between the control conditions with no vibration and antagonist vibration for the entire movement.

This confirms that the initial movement speed correction is a reflexive response to increased type Ia firing, operating well below the time required for conscious and deliberate motor control. In the context of Active Inference, such adjustments would reflect actions aimed at minimizing proprioceptive prediction error, effectively aligning actual sensory feedback with predicted sensory consequences of movement (Friston et al., 2010). From a signal-dependent noise perspective, corrections may be seen as restoring or replanning a trajectory that best minimizes endpoint variance (Harris & Wolpert, 1998).

We generally observed a similar, although slightly longer (approximately 59 ms) and more variable delay to turning off the antagonist vibration until movement speed was increased in response. This

may be due to a limitation in our implementation of vibration motor control; while the vibration motor was always in a consistent state at vibration start (non-vibrating), the state of the motor was variable when vibration stop was triggered, such that it might either be accelerating towards or away from the antagonist muscle when power was cut. Given that the length of a single oscillatory cycle exceeds the estimated difference (a single cycle lasts 12.5 ms for an 80 Hz signal), and that it likely takes some small amount of time for the moving motor to dissipate its energy from when power is cut, the actual physiological delay is likely very similar.

5.4 Limitations & concluding remarks

In this study, we approached the investigation of muscle vibration through the lens of active self-paced movements, with arm movement restricted to the elbow joint only. This approach has the advantage of simplifying the assumptions regarding the effects of muscle vibration on perceived joint angles and velocities. However, with both the biceps and triceps brachii crossing both the elbow and shoulder joint, any bias introduced in the firing rate of muscle afferents here would presumably influence both the perceived elbow and shoulder state. This significantly increases the complexity of forming hypotheses regarding the expected movement corrections in response to muscle vibration for whole-arm movement. While the current approach with restricted movement sidesteps this issue to some extent, it has drawbacks in terms of generalizing our observations to more natural whole-arm/body movement. A limitation here is that 1-dimensional movement, as is the case here, limits endpoint errors to lie along this dimension exclusively. Additional freedom of movement dimensions may be necessary to fully describe whether muscle vibration increases variation in endpoint errors, even if this effect is not apparent with the current setup.

Further, our discussion was framed mostly based on the effects of antagonist muscle vibration, while we tested the impact of both agonist and antagonist vibration. Generally, for agonist vibration, we saw effects in the opposite direction, although smaller and less consistent. This generally matches well with previous research (Capaday & Cooke, 1981, 1983; Cody et al., 1990; Inglis & Frank, 1990; Macefield & Knellwolf, 2018), although our results do expand on the earlier findings, as we did observe consistent effects on the actual movement speed in both Tasks 1 and 2. In Task 2, we found no indication of any interaction effect between the vibration motors, indicating that the combined effect of both vibration motors on both perception of arm position and velocity is well approximated by the sum of each vibration motor alone. Together, this suggests that state estimation during active movement is based on feedback from both the agonist and antagonist muscles, as previously demonstrated in passive conditions (Gilhodes et al., 1986).

In summary, our results suggest that the perception of limb position and velocity is an integrated process, with sensed limb velocity likely contributing to the perceived limb position through an integral-like computation of the velocity signal. A mechanism for such velocity-to-position estimation arises naturally within predictive frameworks of sensori-motor control, such as Active Inference and Optimal Feedback Control (Wolpert et al., 1995; Friston et al., 2010). To the extent that velocity signals contribute to position estimation via an integration-like process, it is equally plausible that position signals could influence velocity estimation through a differentiation-like mechanism, although this was not investigated here. Such reciprocal interactions in state estimation would serve to maintain a stable and self-consistent representation of limb state across both position and velocity domains, with the unavoidable downside that any sensory error in one domain would have downstream effects on the other domain as well, as demonstrated through the application of muscle vibration here. While the

observed movement speed corrections are too fast to be deliberately driven, the underlying perceived bias in movement speed is nevertheless available for verbal report.

To reach out and grasp an object, we must infer our own body position and movement kinematics. This study provides further support for predictive models of sensory integration and motor control, demonstrating that limb state estimation is an integrated process spanning both position and velocity domains.

6 Additional Information

6.1 Data availability

The source data and analysis code will be made publicly available at the time of peer-review publication.

6.2 Grants

This project was supported by a DATA+ grant from UCPH. MSC was supported by DFF-FKK (0132-00141B) and the Carlsberg Foundation (CF22-0941).

6.3 Disclosures

The authors report no conflicts of interest.

6.4 Author contributions

The experiment was conducted at the Cognition, Intention and Action research group, Section for Cognition and Neuropsychology, Department of Psychology, University of Copenhagen, Øster Farimagsgade 2A, Copenhagen.

ESM and MSC conceptualized and designed the research project. ESM acquired and analyzed the data and drafted the manuscript, and ESM and MSC revised and edited the manuscript. ESM and MSC confirm that they have read and approved the final version of the manuscript.

6.5 Acknowledgments

The authors would like to thank Mantas Cibulskis, Difeng Yu, and Joanna Emilia Bergström for their valuable discussions and insights on the topic of sensory inference.

6.6 Keywords

sensorimotor control, sensory integration, muscle tendon vibration, Ia afferent, position estimation, velocity estimation

References

Matthews, P. B. (1963). The response of de-efferented muscle spindle receptors to stretching at different velocities. *The Journal of Physiology*, *168*(3), 660. https://doi.org/10.1113/JPHYSIOL.1963.SP007214

Eklund, G. (1972). Position sense and state of contraction; the effects of vibration. *Journal of Neurology, Neurosurgery & Psychiatry*, *35*(5), 606–611. https://doi.org/10.1136/jnnp.35.5.606

Goodwin, G. M., McCloskey, D. I., & Matthews, P. B. C. (1972). Proprioceptive Illusions Induced by Muscle Vibration: Contribution by Muscle Spindles to Perception? *Science*, *175*(4028), 1382–1384. https://doi.org/10.1126/science.175.4028.1382

Capaday, C., & Cooke, J. D. (1981). The Effects of Muscle Vibration on the Attainment of Intended Final Position During Voluntary Human Arm Movements*. *Experimental Brain Research*, *42*(42), 228–230. https://doi.org/10.1007/BF00236912

Roll, J. P., & Vedel, J. P. (1982). Kinaesthetic Role of Muscle Afferents in Man, Studied by Tendon Vibration and Microneurography. *Experimental Brain Research*, *47*(2), 177–190. https://doi.org/10.1007/BF00239377

Capaday, C., & Cooke, J. D. (1983). Vibration-induced changes in movement-related EMG activity in humans. *Experimental Brain Research*, *52*(1), 139–146. https://doi.org/10.1007/BF00237158

Gilhodes, J., Roll, J., & Tardy-Gervet, M. (1986). Perceptual and motor effects of agonist-antagonist muscle vibration in man. *Experimental Brain Research*, *61*(2), 395–402. https://doi.org/10.1007/BF00239528

Roll, J. P., Vedel, J. P., & Ribot, E. (1989). Alteration of proprioceptive messages induced by tendon vibration in man: a microneurographic study. *Experimental Brain Research*, *76*(76), 213–222. https://doi.org/10.1007/BF00253639

Yamamoto, C., & Ohtsuki, T. (1989). Modulation of stretch reflex by anticipation of the stimulus through visual information. *Experimental Brain Research*, *77*(1), 12–22. https://doi.org/10.1007/BF00250562

Cody, F. W., Schwartz, M. P., & Smit, G. P. (1990). Proprioceptive guidance of human voluntary wrist movements studied using muscle vibration. *The Journal of Physiology*, *427*(1), 455–470. https://doi.org/10.1113/jphysiol.1990.sp018181

Inglis, J. T., & Frank, J. S. (1990). The effect of agonist/antagonist muscle vibration on human position sense. *Experimental Brain Research*, *81*(3), 573–580. https://doi.org/10.1007/BF02423506

Carlin, B. P., Gelfand, A. E., & Smith, A. F. M. (1992). Hierarchical Bayesian Analysis of Changepoint Problems. *Journal of the Royal Statistical Society: Series C (Applied Statistics)*, *41*(2), 389–405. https://doi.org/10.2307/2347570

Rossetti, Y., Stelmach, G., Desmurget, M., Prablanc, C., & Jeannerod, M. (1994). The effect of viewing the static hand prior to movement onset on pointing kinematics and variability. *Experimental brain research*, *101*(2), 323–330. https://doi.org/10.1007/BF00228753

Rossetti, Y., Desmurget, M., & Prablanc, C. (1995). Vectorial Coding of Movement: Vision, Proprioception, or Both? *Journal of Neurophysiology*, *74*(1), 457–463. https://doi.org/10.1152/jn.1995.74.1.457

Wolpert, D. M., Ghahramani, Z., & Jordan, M. I. (1995). An internal model for sensorimotor integration. *Science*, *269*(5232), 1880–1882. https://doi.org/10.1126/SCIENCE.7569931,

Desmurget, M., Rossetti, Y., Jordan, M., Meckler, C., & Prablanc, C. (1997). Viewing the hand prior to movement improves accuracy of pointing performed toward the unseen contralateral hand. *Experimental Brain Research*, *115*(1), 180–186. https://doi.org/10.1007/PL00005680

Nakazawa, K., Yamamoto, S.-i., & Yano, H. (1997). Short- and long-latency reflex responses during different motor tasks in elbow flexor muscles. *Experimental Brain Research*, (116), 20–28. https://doi.org/10.1007/pl00005740

Harris, C. M., & Wolpert, D. M. (1998). Signal-dependent noise determines motor planning. *Nature*, *394*(6695), 780–784. https://doi.org/10.1038/29528;KWRD=SCIENCE

Todorov, E., & Jordan, M. I. (1998). Smoothness maximization along a predefined path accurately predicts the speed profiles of complex arm movements. *Journal of Neurophysiology*, *80*(2), 696–714. https://doi.org/10.1152/JN.1998.80.2.696,

Calvin-Figuière, S., Romaiguère, P., Gilhodes, J. C., & Roll, J. P. (1999). Antagonist motor responses correlate with kinesthetic illusions induced by tendon vibration. *Experimental Brain Research*, *124*(3), 342–350. https://doi.org/10.1007/s002210050631

Todorov, E., & Jordan, M. I. (2002). Optimal feedback control as a theory of motor coordination. *Nature Neuroscience*, *5*(11), 1226–1235. https://doi.org/10.1038/NN963;KWRD=BIOMEDICINE

Van Beers, R. J., Baraduc, P., & Wolpert, D. M. (2002). Role of uncertainty in sensorimotor control. *Philosophical Transactions of the Royal Society B: Biological Sciences*, *357*(1424), 1137–1145. https://doi.org/10.1098/RSTB.2002.1101

Roll, J. P., Albert, F., Ribot-Ciscar, E., & Bergenheim, M. (2004). "Proprioceptive signature" of cursive writing in humans: A multi-population coding. *Experimental Brain Research*, *157*(3), 359–368. https://doi.org/10.1007/s00221-004-1853-x

Albert, F., Bergenheim, M., Ribot-Ciscar, E., & Roll, J. P. (2006). The Ia afferent feedback of a given movement evokes the illusion of the same movement when returned to the subject via muscle tendon vibration. *Experimental Brain Research*, *172*(2), 163–174. https://doi.org/10.1007/s00221-005-0325-2

Bock, O., Pipereit, K., & Mierau, A. (2007). A method to reversibly degrade proprioceptive feedback in research on human motor control. *Journal of Neuroscience Methods*, *160*(2), 246–250. https://doi.org/10.1016/j.jneumeth.2006.09.010

Dimitriou, M., & Edin, B. B. (2008). Discharges in human muscle spindle afferents during a key-pressing task. *The Journal of Physiology*, *586*(22), 5455–5470. https://doi.org/10.1113/JPHYSIOL.2008.160036

Kurtzer, I. L., Pruszynski, J. A., & Scott, S. H. (2008). Long-Latency Reflexes of the Human Arm Reflect an Internal Model of Limb Dynamics. *Current Biology*, *18*(6), 449–453. https://doi.org/10.1016/j.cub.2008.02.053

Friston, K. J., Daunizeau, J., Kilner, J., & Kiebel, S. J. (2010). Action and behavior: A free-energy formulation. *Biological Cybernetics*, *102*(3), 227–260. https://doi.org/10.1007/s00422-010-0364-z

Proske, U., & Gandevia, S. C. (2012). The Proprioceptive Senses: Their Roles in Signaling Body Shape, Body Position and Movement, and Muscle Force. *Physiol Rev*, *92*, 1651–1697. https://doi.org/10.1152/physrev.00048.2011

Kurtzer, I. L. (2015). Long-latency reflexes account for limb biomechanics through several supraspinal pathways. *Frontiers in Integrative Neuroscience*, *8*(JAN), 1–19. https://doi.org/10.3389/fnint.2014.00099

Chancel, M., Blanchard, C., Guerraz, M., Montagnini, A., & Kavounoudias, A. (2016). Optimal visuo-tactile integration for velocity discrimination of self-hand movements. *Journal of Neurophysiology*, *116*(3), 1522–1535. https://doi.org/10.1152/jn.00883.2015

Bürkner, P. C. (2017). brms: An R package for Bayesian multilevel models using Stan. *Journal of Statistical Software*, *80*. https://doi.org/10.18637/jss.v080.i01

Patterson, J. R., Brown, L. E., Wagstaff, D. A., & Sainburg, R. L. (2017). Limb position drift results from misalignment of proprioceptive and visual maps. *Neuroscience*, *346*, 382–394. https://doi.org/10.1016/J.NEUROSCIENCE.2017.01.040

Macefield, V. G., & Knellwolf, T. P. (2018). Functional properties of human muscle spindles. *Journal of Neurophysiology*, *120*(2), 452–467. https://doi.org/10.1152/jn.00071.2018

Ferrari, F., Clemente, F., & Cipriani, C. (2019). The preload force affects the perception threshold of muscle vibration-induced movement illusions. *Experimental Brain Research*, *237*(1), 111–120. https://doi.org/10.1007/s00221-018-5402-4

Keyser, J., Ramakers, R. E., Medendorp, W. P., & Selen, L. P. (2019). Task-dependent responses to muscle vibration during reaching. *European Journal of Neuroscience*, *49*(11), 1477–1490. https://doi.org/10.1111/ejn.14292

Wickham, H., Averick, M., Bryan, J., Chang, W., McGowan, L., François, R., Grolemund, G., Hayes, A., Henry, L., Hester, J., Kuhn, M., Pedersen, T., Miller, E., Bache, S., Müller, K., Ooms, J., Robinson, D., Seidel, D., Spinu, V., … Yutani, H. (2019). Welcome to the Tidyverse. *Journal of Open Source Software*, *4*(43), 1686. https://doi.org/10.21105/joss.01686

Brookes, J., Warburton, M., Alghadier, M., Mon-Williams, M., & Mushtaq, F. (2020). Studying human behavior with virtual reality: The Unity Experiment Framework. *Behavior Research Methods*, *52*(2), 455–463. https://doi.org/10.3758/s13428-019-01242-0

Abril-Pla, O., Andreani, V., Carroll, C., Dong, L., Fonnesbeck, C. J., Kochurov, M., Kumar, R., Lao, J., Luhmann, C. C., Martin, O. A., Osthege, M., Vieira, R., Wiecki, T., & Zinkov, R. (2023). PyMC: a modern, and comprehensive probabilistic programming framework in Python. *PeerJ Computer Science*, *9*, e1516. https://doi.org/10.7717/peerj-cs.1516

Chancel, M., & Ehrsson, H. H. (2023). Proprioceptive uncertainty promotes the rubber hand illusion. *Cortex*, *165*, 70–85. https://doi.org/10.1016/j.cortex.2023.04.005

Python Software Foundation. (2023). Python. https://www.python.org

R Core Team. (2024). R: A Language and Environment for Statistical Computing. https://www.R-project.org/

Stan Development Team. (2024). Stan Modeling Language Users Guide and Reference Manual. https://mc-stan.org

7 Appendix

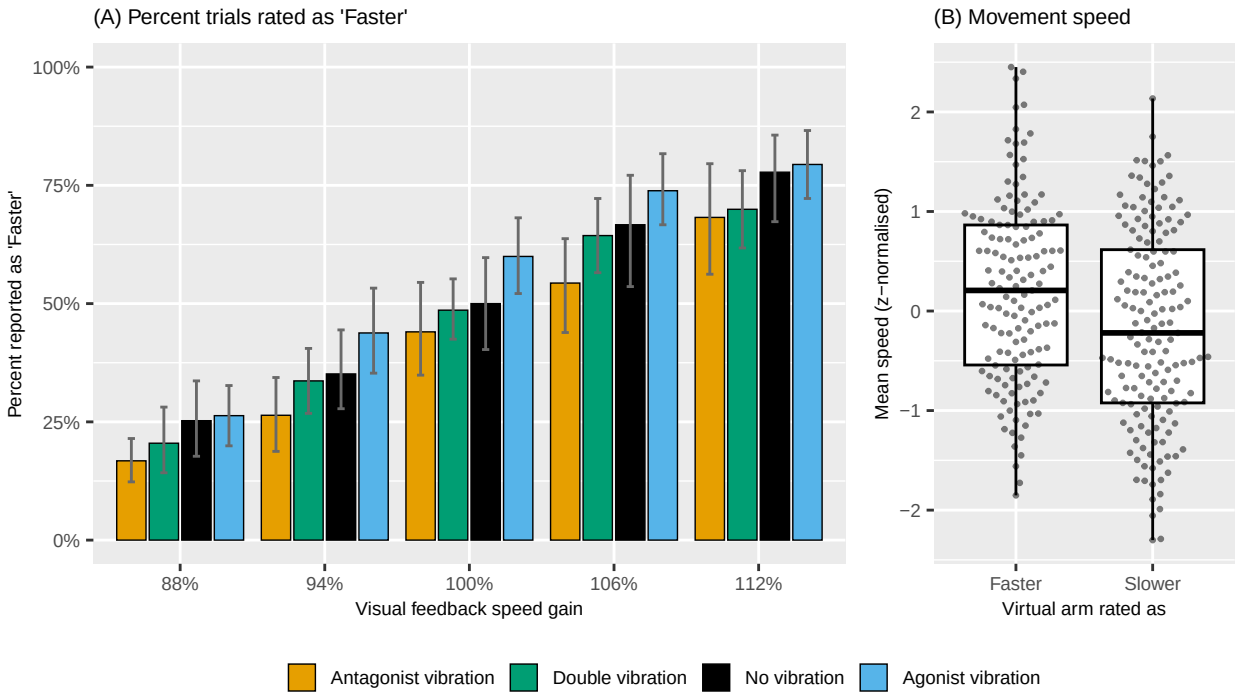

Figure A1: Panel A shows the mean and 95% bootstrapped confidence intervals of subject percentages of trials reported as 'Faster' from Task 1, complement of Figure 2A. Panel B shows z-normalized (within-subject) mean movement speed by subject rating of 'Faster' and 'Slower' from Task 1 trials with no visual speed gain (normal speed) and no vibration, complement of figure 5B.

Outcome	Movement direction	Mean of subject means	Mean of subject SDs
Endpoint error (°)	Extension	-3.28 (5.07)	3.65 (1.05)
Endpoint error (°)	Flexion	-1.12 (3.49)	3.69 (0.96)
Mean movement speed (°/s)	Extension	40.92 (9.83)	7.73 (2.57)
Mean movement speed (°/s)	Flexion	38.55 (7.6)	6.59 (1.74)
Movement time (s)	Extension	1.46 (0.34)	0.29 (0.09)
Movement time (s)	Flexion	1.61 (0.3)	0.29 (0.1)

Table A1: Summary of mean (SD) endpoint errors, mean movement speed, and movement time in Task 2 for the baseline trials with no muscle vibration, along with within-and between-subject variability.

Model A1 describes the complete changepoint model, which was implemented in PyMC. See Figure A2 for a visualization of the fitting process.

The changepoint model approximates the delta mean movement as two linear functions, one before the effect of starting/stopping the vibration motor takes effect, with a slope of near 0, and one after, where the slope will indicate the estimated relative change in velocity over time, i.e., acceleration. These assumptions allow us to sample the most likely changepoints (τ) during model fitting. The same model, using identical priors, is fit twice, once for detecting the latency of turning on the vibration motor until velocity is changed, and once for turning off. dms_i is the movement speed difference at time t_i (in deg/s). Specifically, it is calculated by subtracting the mean speed of the control condition from each observation in the intervention condition (within-participant) at time t_i. A sigmoid function (S_i) with a very rapid transition between asymptotic values is used to blend between the two linear functions. The estimated inflection point τ thus models the latency. Zero-centered priors are used for the slopes both pre and post τ, and a uniform prior was used for the value of τ between 0 (vibration start/stop) and the max time stamp of the included data (120 ms after vibration start/stop).

The model definition is subdivided into the likelihood function, as well as priors, which here describe the subject-level parameters (random effects, marked as j), and the hyperpriors, which represent the priors of the group-level parameters (fixed effects). The distribution of subject-level parameters is modeled as Gaussian distributions centered on the group means (marked with overlines), e.g., subject changepoints are assumed to be normally distributed. We use an uncentered parameterization of the model here to aid convergence. This relates to parameters marked as ϵ; including these ϵ terms significantly improves sampling efficiency and convergence.

dms_i are at t_i modeled as a Gaussian distribution with μ_i and σ_j. μ_i is a blend between the two linear functions, $\mu_pre_\tau_i$, $\mu_post_\tau_i$, blended using the value of a sigmoid function (S_i) at t_i. Of note, $\alpha_post_\tau_j$ is defined deterministically depending on the sampled values of $\alpha_pre_\tau_j$, $\beta_pre_\tau_j$, $\beta_post_\tau_j$ and τ_j, such that the two linear functions intersect at $t = \tau_j$. This ensures continuity between $\mu_pre_\tau_i$ and $\mu_post_\tau_i$ within each set of sampled values. For simplicity, the distribution of observed dms_i is assumed to be constant across values of t_i, within-subject (denoted by σ_j).

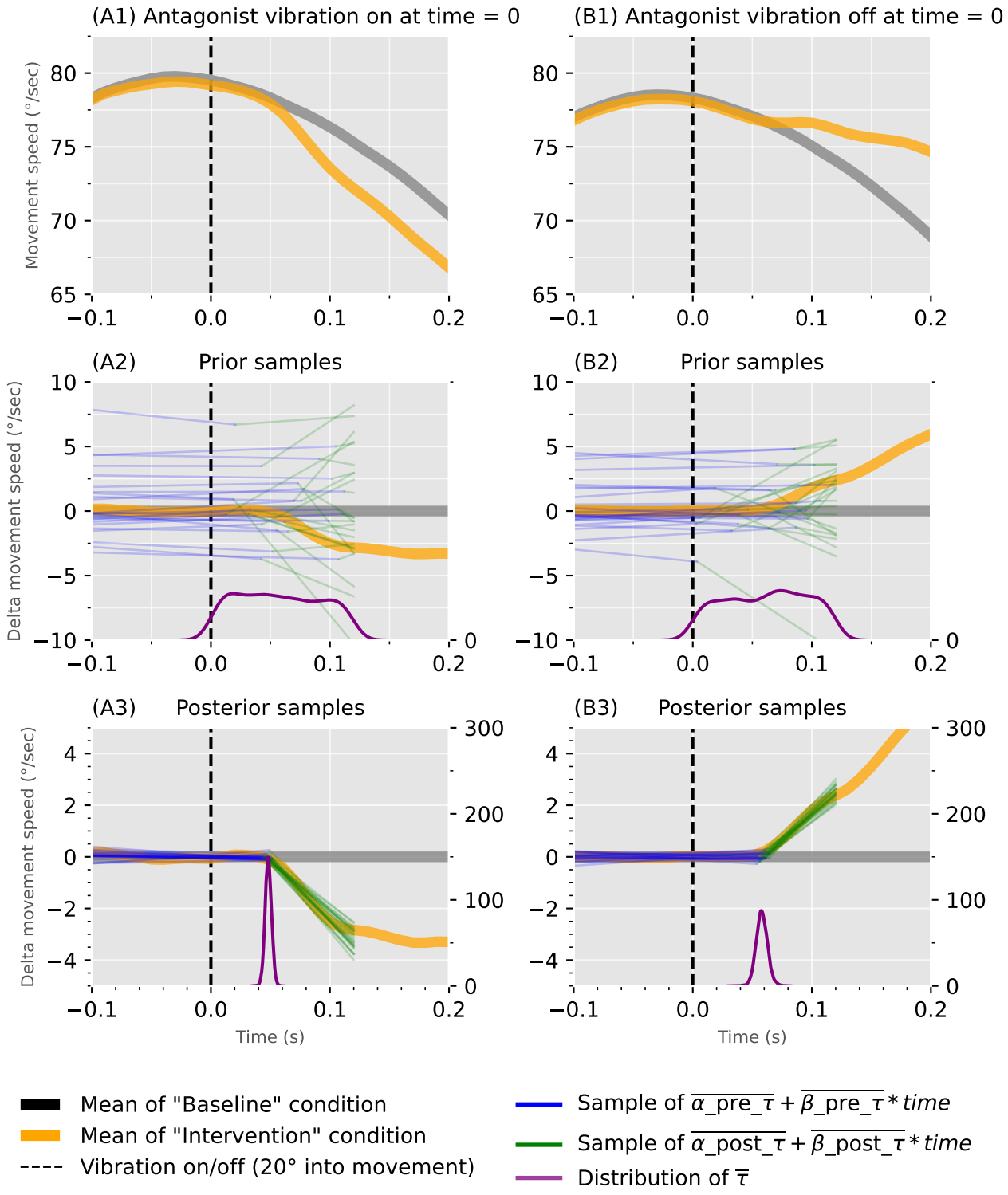

Figure A2: Visualizes the fitting process of model A1. Panels A1 and B1 show the mean movement speed of the two sets of intervention and control conditions, with control conditions in grey and intervention conditions in orange. Panels A2 and B2 display the same two lines, with the mean of the control condition subtracted from its corresponding intervention condition trials at each time point t. As a result, the orange line now represents the delta mean movement speed between the two conditions. A subset of prior draws of the pre- and post- $\overline{\tau}$ linear function parameters (blue and green), as well as the prior distribution of $\overline{\tau}$ (purple), are also shown. Panels A3 and B3 show a subset of posterior draws of the two linear function parameters and the posterior distribution of $\overline{\tau}$. Note that while only the across-subjects mean delta movement speed is shown (orange), the model is fitted to the underlying trial-level data in a hierarchical fashion to account for subject-to-subject variation.

$$
\begin{aligned}
&\textbf{Likelihood} \\
dms_i &\sim \mathcal{N}(\mu_i, \sigma_j) \\
\mu_i &= \mu_pre_\tau_i \cdot S_i + \mu_post_\tau_i \cdot (1 - S_i) \\
S_i &= \frac{1}{1 + e^{\frac{t_i - \tau_j}{0.001}}} \\
\mu_pre_\tau_i &= \alpha_pre_\tau_j + \beta_pre_\tau_j \cdot t_i \\
\mu_post_\tau_i &= \alpha_post_\tau_j + \beta_post_\tau_j \cdot t_i \\
&\textbf{Priors} \\
\alpha_pre_\tau_j &= \overline{\alpha_pre_\tau} + \alpha_pre_\tau_\sigma \cdot \epsilon_\alpha_pre_\tau_j && \text{for } j \in \{1, \ldots, n_{id}\} \\
\epsilon_\alpha_pre_\tau_j &\sim \mathcal{N}(0, 1) && \text{for } j \in \{1, \ldots, n_{id}\} \\
\beta_pre_\tau_j &= \overline{\beta_pre_\tau} + \beta_pre_\tau_\sigma \cdot \epsilon_\beta_pre_\tau_j && \text{for } j \in \{1, \ldots, n_{id}\} \\
\epsilon_\beta_pre_\tau_j &\sim \mathcal{N}(0, 1) && \text{for } j \in \{1, \ldots, n_{id}\} \\
\beta_post_\tau_j &= \overline{\beta_post_\tau} + \beta_post_\tau_\sigma \cdot \epsilon_\beta_post_\tau_j && \text{for } j \in \{1, \ldots, n_{id}\} \\
\epsilon_\beta_post_\tau_j &\sim \mathcal{N}(0, 1) && \text{for } j \in \{1, \ldots, n_{id}\} \\
\alpha_post_\tau_j &= \alpha_pre_\tau_j + (\beta_pre_\tau_j - \beta_post_\tau_j \cdot \tau_j) && \text{for } j \in \{1, \ldots, n_{id}\} \\
\tau_j &= \overline{\tau} + \tau_\sigma \cdot \epsilon_\tau_j && \text{for } j \in \{1, \ldots, n_{id}\} \\
\epsilon_\tau_j &\sim \mathcal{N}(0, 1) && \text{for } j \in \{1, \ldots, n_{id}\} \\
\sigma_j &= \frac{1}{1 + e^{\sigma_log_j}} && \text{for } j \in \{1, \ldots, n_{id}\} \\
\sigma_log_j &= \overline{\sigma_log} + \sigma_log_\sigma \cdot \epsilon_\sigma_log_j && \text{for } j \in \{1, \ldots, n_{id}\} \\
\epsilon_\sigma_log_j &= \mathcal{N}(0, 1) && \text{for } j \in \{1, \ldots, n_{id}\} \\
&\textbf{Hyperpriors} \\
\overline{\alpha_pre_\tau} &\sim \mathcal{N}(0, 2.5) \\
\alpha_pre_\tau_\sigma &\sim \mathrm{HN}(5) \\
\overline{\beta_pre_\tau} &\sim \mathcal{N}(0, 5) \\
\beta_pre_\tau_\sigma &\sim \mathrm{HN}(5) \\
\overline{\beta_post_\tau} &\sim \mathcal{N}(0, 50) \\
\beta_post_\tau_\sigma &\sim \mathrm{HN}(25) \\
\overline{\tau} &\sim \mathcal{U}(0, t_{max}) \\
\tau_\sigma &\sim \mathrm{HN}(0.025) \\
\overline{\sigma_log} &\sim \mathcal{N}(0, 10) \\
\sigma_log_\sigma &\sim \mathrm{HN}(10)
\end{aligned}
\tag{A1}
$$